ADVANCED FUNCTIONAL MATERIALS
www.afm-journal.de

Materials Views
www.MaterialsViews.com

Hierarchical Y and USY Zeolites Designed by Post-Synthetic Strategies

*Danny Verboekend, Gianvito Vilé, and Javier Pérez-Ramírez**

Strategic combinations of affordable and scalable post-synthetic modifications enabled to design a broad family of hierarchical Y and USY zeolites (FAU topology) independent on the Si/Al ratio. Pristine (Y, Si/Al = 2.4), steamed (USY, Si/Al = 2.6), and steamed and dealuminated (USY, Si/Al = 15 and 30) zeolites were exposed to a variety of acid (H_4EDTA and Na_2H_2EDTA) and base (NaOH) treatments, which led to the introduction of mesopore surfaces up to 500 $m^2\ g^{-1}$, while preserving the intrinsic zeolite properties. Pristine Y and USY zeolites (Si/Al ~ 2.5) required mild dealumination (to Si/Al > 4 in the case of Y) to facilitate subsequent efficient desilication. Alkaline treatment of Y and USY zeolites with low Si/Al ratios (~4–6) led to an abundance of Al-rich debris, which could be removed by a subsequent mild acid wash. On the other hand, severely steamed and dealuminated, hence Si-rich, USY zeolites (Si/Al = 15 and 30) proved extremely sensitive to the alkaline solution, displaying facile dissolution and substantial amorphization. For the latter group of ultra-stable Y zeolites, the presence of TPA^+ in the alkaline solution enables to protect the zeolite structures upon the introduction of mesoporosity by desilication, preserving crystallinity and micropore volume. The sorption and catalytic properties of the hierarchical Y and USY zeolites were superior compared to the conventional counterparts.

1. Introduction

Zeolite catalysts are of eminent importance in a number of chemical reactions associated with the (petro)chemical and oil refining industries,[1,2] and raise substantial interest in new applications, such as the conversion of biomass into valuable chemicals.[3,4] Nevertheless, especially during the processing of bulky molecules in the liquid phase, a sub-optimal utilization of the active sites present in zeolites is often implied by limited access and slow intra-crystalline diffusion in their micropores.[5] In response to the need of improved catalytic processes, hierarchical (mesoporous) zeolites have been conceived. These modified zeolites integrate the native microporosity with an auxiliary level of inter or intra-crystalline mesopores, increasing the external surface area substantially. This brings enhanced accessibility due to the increased number of pore mouths and shortened average diffusion pathlength in the micropores.[6–9] The superior lab-scale performance of hierarchical zeolites compared to conventional counterparts in a wide range of catalyzed reactions is unquestionable.

Currently, a varied assortment of top-down and bottom-up approaches is available to synthesize hierarchically structured zeolites.[10–14] The synthetic elegance of bottom-up methods is counteracted by a low chance for industrialization, since they commonly necessitate the use of costly and commercially unavailable reactants as mesopore-inducing agents,[15–19] and/or lead to products not easily separated from the mother liquor, e.g., nano-crystals or nano-sheets.[19,20] On the other hand, top-down approaches such as demetallation are highly effective and scalable at a reasonable cost. As a matter of fact, post-synthetic modifications are largely responsible for the success of zeolites in general, yielding superior catalysts in terms of stability, composition, and acid site speciation.[2] The best example, applied in industry since the 60s, is the stabilization of Y zeolite by steam treatment,[21–24] whereas acid treatments are routinely applied by zeolite producers to remove extra-framework aluminum.[23,24]

Stabilization of the pristine Y zeolite (FAU topology)[25] by framework dealumination is commonly performed, since its high framework Al content renders it unstable once brought in the protonic form. The ultra-stable derivative (zeolite USY) is widely used in industry for fluid catalytic cracking and hydrocracking,[2,7] and a generalized protocol to synthesize hierarchical analogues would be of prominent value because of the relatively bulky hydrocarbons involved and the need to control selectivity and to increase lifetime. The dealumination of the framework can, besides increasing (hydro)thermal stability, also lead to the introduction of a secondary network of mesopores in the zeolite crystal.[7,24,26] Nevertheless, in the case of steam treatment, the formed mesopores do not significantly affect intra-crystalline diffusion of probe molecules,[27] since they are mostly present as cavities.[28] In the last decade, base leaching, known as desilication, has become a widely-applied post-synthetic treatment, since it enables to introduce a network of connected intra-crystalline mesopores, while conserving the intrinsic zeolite properties.[14,29] Desilication has been routinely applied to

D. Verboekend, G. Vilé, Prof. J. Pérez-Ramírez
Institute for Chemical and Bioengineering
Department of Chemistry and Applied Biosciences
ETH Zurich, Wolfgang-Pauli-Strasse 10
CH 8093, Zurich, Switzerland
E-mail: jpr@chem.ethz.ch

DOI: 10.1002/adfm.201102411

introduce a secondary network of mesopores in multiple high-silica frameworks in the Si/Al range 10 to infinite.[14,30,31] However, alkaline treatment on zeolites with high Al content (Si/Al ratio < 10) remains relatively unexplored.

Two recent papers revealed the main challenges in the preparation of hierarchical Y and USY by desilication. Qin et al.[32] performed severe alkaline treatments (368 K, 0.5–1.3 M NaOH, 1–3 h) on a pristine zeolite Y (mesopore surface area = 18 $m^2\ g^{-1}$, Si/Al = 3.1), but obtained a limited mesoporosity (S_{meso} = 61 $m^2\ g^{-1}$), whereas crystallinity remained mostly unchanged. On the contrary, de Jong et al.[33] performed alkaline treatments on a severely steamed and acid-leached zeolite USY (S_{meso} = 213 $m^2\ g^{-1}$, Si/Al = 28). They used very mild conditions (298 K, 0.05–0.1 M NaOH, 15 min) to develop impressive external surfaces up to 443 $m^2\ g^{-1}$. However, the resulting zeolite displayed a strong amorphization, substantiated by the two-third reduction in micropore volume (from 0.21 $cm^3\ g^{-1}$ down to 0.07 $cm^3\ g^{-1}$) and crystallinity. Although these works clearly prove that Y and severely-steamed and dealuminated USY behave very distinctly in alkaline media, no general knowledge for the precise manipulation of the FAU framework exists thus far.

Herein, we present combinations of acid and base treatments to prepare hierarchical Y and USY zeolites. The selection of different starting zeolites combined with a comprehensive set of post-synthetic modifications enabled to substantiate the contradictory relationship between the sensitive FAU framework and its high Al content. We identify a critical Si/Al ratio above which the facile dissolution by alkaline treatment and introduction of external surface occurs. Besides, we highlight the necessity to remove debris from zeolites after acid or alkaline treatment to fully exploit the intrinsic and the newly developed properties in adsorption and/or catalysis. In the case of severely dealuminated USY zeolites, it is demonstrated that the inclusion of tetraalkalyammonium cations in the base solution enables to introduce substantial mesoporosity, while maintaining the intrinsic zeolite properties. The superiority of hierarchical Y and USY is evidenced in the adsorption of toluene, the alkylation of benzyl alcohol with toluene, and the pyrolysis of polyethylene. In an exciting culmination to recent studies on MFI, this work extrapolates gained insights into the FAU framework, and provides post-synthetic strategies to the synthesis of mesoporous zeolites.

2. Results and Discussion

The commercial zeolites used as starting materials for the post-synthetic treatments comprised a parent Y (Si/Al = 2.4), a mildly steamed USY (Si/Al = 2.6), and two severely steamed and acid-leached USY zeolites (Si/Al = 15 and 30). Acid treatments performed comprised aqueous solutions of ethylenediaminetetraacetic acid (H_4EDTA) and ethylenediamine-tetraacetic acid disodium salt (Na_2H_2EDTA), whereas base treatments were performed using aqueous NaOH in the absence or presence of tetrapropylammonium cations (TPA^+). The majority of the study focuses on Y zeolite (Si/Al = 2.4), which is described in Sections 2.1-2.5. Results derived from treatments of the USY zeolites are described in Section 2.6. A general discussion on strategies to design hierarchical Y and USY zeolites is provided in Section 2.7.

2.1. Individual Acid and Base Treatments on Zeolite Y

The parent sample (P, Si/Al = 2.4) comprised octahedron-type crystals typical for the faujasite zeolite.[28] TEM showed that the crystals were free of intra-crystalline defects (**Figure 1**), while

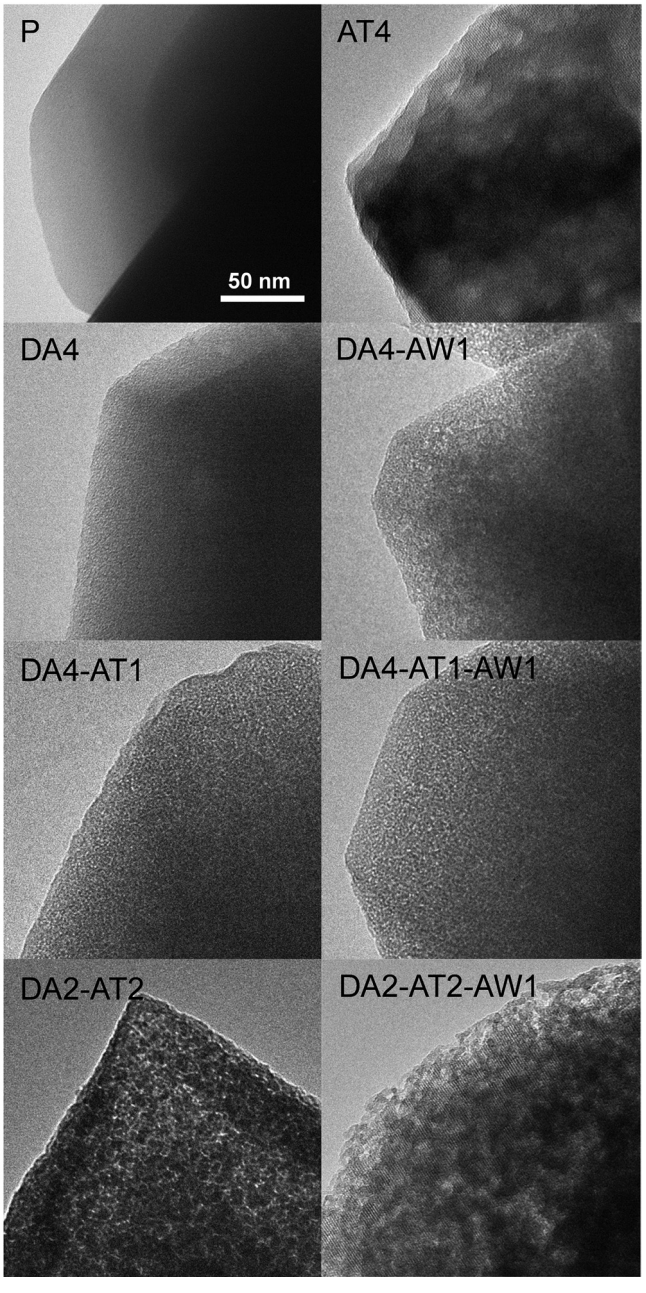

Figure 1. Transmission electron microscopy images of Y zeolites at different stages of the treatment sequence. The scale bar applies to all images. The mesopores are typically homogenously distributed and mostly intra-crystalline.

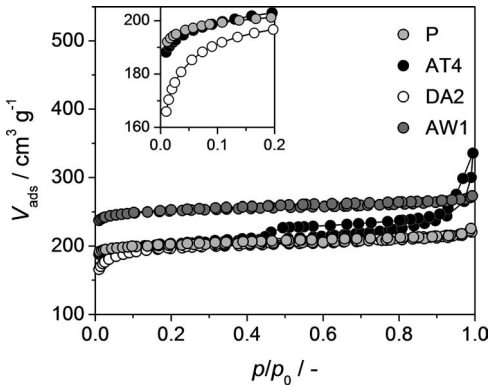

Figure 2. N_2 isotherms at 77 K of Y zeolites after individual treatment with NaOH (AT4), H_4EDTA (DA2), and Na_2H_2EDTA (AW1). The inset highlights the uptake at low relative pressures. The individual treatments did not yield Y zeolites with significant mesoporosity.

Table 1. Notation of the samples and treatment conditions.

Sample code	Reagent	*C* [M]	*T* [K]	*t* [h]
DA1	H_4EDTA	0.07	373	6
DA2	H_4EDTA	0.11	373	6
DA3	H_4EDTA	0.15	373	6
DA4	H_4EDTA	0.11	373	72
AT1	NaOH	0.10	338	0.5
AT2	NaOH	0.20	338	0.5
AT3	NaOH	3.00	338	0.5
AT4	NaOH	5.00	338	0.5
AT1+TPA	NaOH+TPAOH	0.05+0.05	338	0.5
AT2+TPA	NaOH+TPAOH	0.15+0.05	338	0.5
AW1	Na_2H_2EDTA	0.11	373	6

its X-ray diffraction (XRD) pattern revealed a highly crystalline faujasite in the absence of impurities (Supporting Information (SI), Figure SI1). N_2 sorption resulted in a type-I isotherm, typical for purely microporous materials (P in **Figure 2**). Application of the *t*-plot model evidenced a micropore volume (V_{micro}) of 0.30 cm^3 g^{-1} and a limited mesopore surface area (S_{meso}) of 22 m^2 g^{-1}.

Various (individual and sequential) treatments are presented in this paper, ultimately aimed at preparing a superior hierarchical Y zeolite. The individual influence of each treatment on the parent zeolite Y was explored (**Figure 3**). The treatment conditions of representative samples are provided in **Table 1**, whereas a full overview of the treatment conditions and the porosity of the resulting solids is shown in Tables SI1-2.

In line with the low Si/Al ratio of the pristine zeolite, relatively high molarities of aqueous NaOH were required to induce dissolution (Figure 3a). Accordingly, only at 5 M NaOH, yields dropped to ca. 60%, i.e., a value typical for alkaline-treated MFI zeolites.[31] As expected,[32] the alkaline treatments of pristine Y resulted in a minor development of mesoporosity; the highest S_{meso} did not exceed 60 m^2 g^{-1}. Additionally, the N_2 isotherm suggests the presence of macroporosity (Figure 2), which was confirmed by TEM (AT4 in Figure 1). On the other hand, crystallinity remained relatively high (ca. 80%), while V_{micro} remained mostly unchanged. It is likely that the high alkalinities applied led to an unselective dissolution, incapable of directing the silicon leaching process towards the efficient introduction of intra-crystalline mesoporosity.

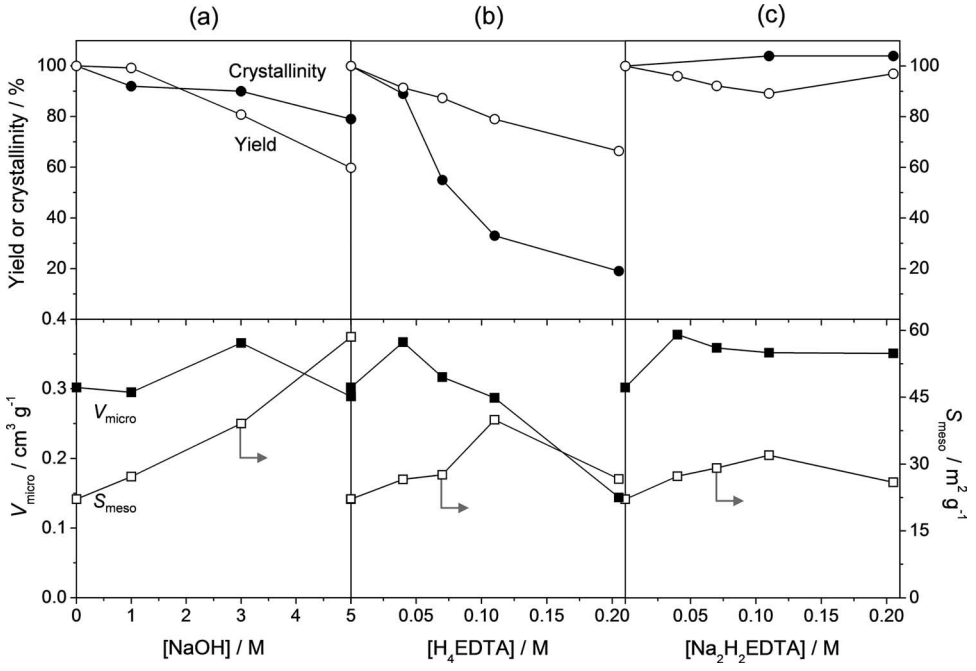

Figure 3. Influence of a) NaOH, b) H_4EDTA, or c) Na_2H_2EDTA treatments on crystallinity (solid circles), yield (open circles), micropore volume (solid squares), and mesopore surface area (open squares) of the Y zeolites. The parent Y zeolite is represented at 0 M.

Aqueous solutions of H_4EDTA were used to dealuminate the Y framework since, compared to mineral acids, it preserves crystallinity to a larger extent.[26] Exposure to aqueous H_4EDTA solutions led to a gradual loss in yields (down to 70% at 0.2 M), while crystallinity reduced strongly (down to ca. 20% at 0.2 M, Figure 3b). The latter can be expected since at 0.2 M H_4EDTA, more than 50% of Al should have been removed from the solid.[34] Even though the framework appeared substantially affected, application of the *t*-plot model to the isotherm did not reveal the loss of micropore volume or the presence of mesopores. However, closer inspection of a representative N_2 isotherm (DA2 in Figure 2) suggested the presence of large micropores or small mesopores. The drop in micropore volume became significant at concentrations exceeding 0.11 M (down to ca. 0.12 $cm^3\ g^{-1}$ at 0.20 M).

Treatment with aqueous Na_2H_2EDTA is commonly used to remove extra-framework Al from steamed USY zeolites.[26,35] It should therefore ideally exert a minor influence on the parent crystals. Figure 3**c** shows that the yields remained fairly high (ca. 90%), even when concentrations up to 0.6 M were employed (Table SI2). On the other hand, crystallinity increased to a *fictitious* 104%, which suggests the removal of some amorphous species. The porous properties of the Na_2H_2EDTA-treated samples corroborated the minor influence of the treatment on the parent zeolite. Accordingly, a representative isotherm revealed a similar trend to that of P (e.g. sample AW1 in Figure 2).

2.2. Sequential Acid and Base Treatments on Zeolite Y

Individual post-synthetic treatments did not succeed in introducing distinctive mesoporosity in parent Y zeolite. An alternative strategy to obtain highly mesoporous Y zeolites concerns the application of sequential alkaline and acid treatments.[31] Hereto the alkaline-treated sample AT4 was washed with Na_2H_2EDTA to obtain AT4-AW1. These efforts, however, did not result into substantial mesoporosity (Table SI3), and confirmed that alkaline treatment alone is not suited to introduce mesoporosity in the pristine Y zeolite.

To study the influence of dealumination prior to desilication, sequential H_4EDTA and NaOH treatments were systematically screened. This approach resulted in an extended matrix of solids, a large number of which being hierarchical porous structures (Table SI4). For clarity, the influence of the sequential treatments on the porous properties is illustrated by the N_2 isotherms of DA1-AT1 and DA2-AT2 (**Figure 4**a,b), and the general trends are discussed in more detail for DA2-AT2. The N_2 isotherm of the latter sample displayed a similar uptake at low relative pressures compared to sample P, which was coupled to an increased uptake at middle-to-high relative pressures. This amounted to a large mesopore surface (330 $m^2\ g^{-1}$) coupled to a microporosity of 0.20 $cm^3\ g^{-1}$ (**Table 2**). Compared to DA2, this represents an 8-fold increase of the external surface area and a the preservation of two-thirds of the micropore volume. The derived mesopore size distribution displayed mesopores centered around 8 nm, whereas contributions at higher mesopores sizes were completely absent. The latter suggests that purely intracrystalline mesopores were formed, which was confirmed by TEM (DA2-AT2 in Figure 1). Surprisingly, although substantial

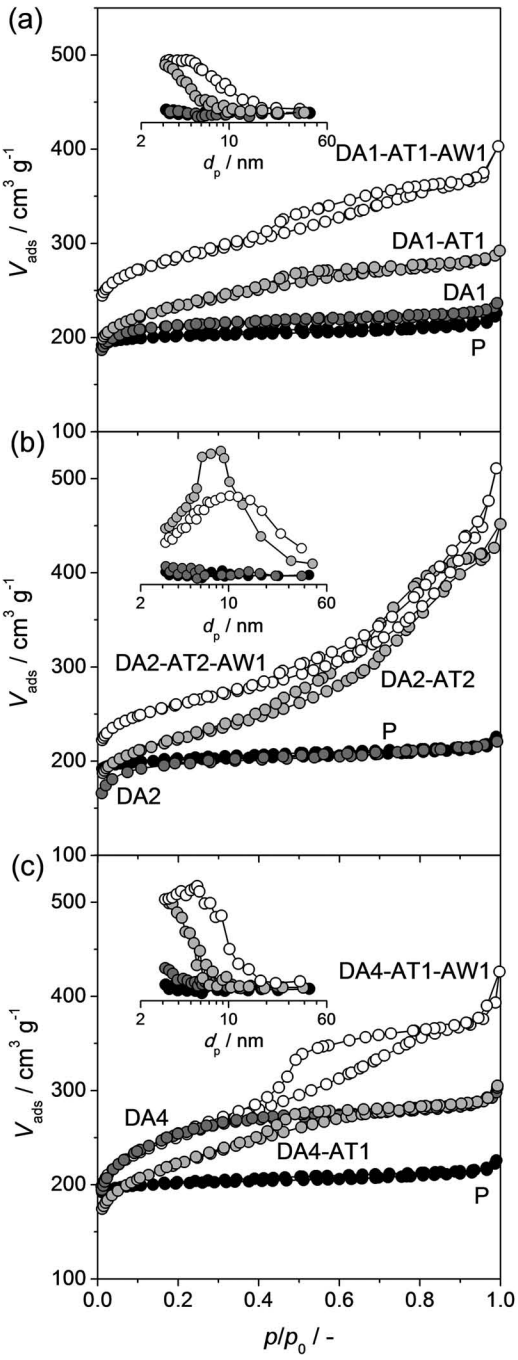

Figure 4. N_2 isotherms at 77 K of the Y zeolites using different sequences. Insets: BJH mesopore size distributions. The post-synthetic modifications resulted in hierarchical Y zeolites with distinct mesopore sizes.

mesoporosity was introduced, crystallinity did not decrease abruptly upon alkaline treatment (from 31% to 18%, **Figure 5**).

The textural parameters collected in Table SI4 were plotted in a number of contour plots to facilitate interpretation. **Figure 6**a shows the overall weight loss upon sequential H_4EDTA and NaOH treatments. The H_4EDTA-treated zeolites (prior to desilication) are represented on the *y*-axis, whereas the *x*-axis depicts the zeolites treated in NaOH only. In agreement with

Table 2. Treatment yields and properties of Y zeolites.

Sample	Yield[a] [%]	Crystallinity[b] [%]	Si/Al[c]	V_{pore}[d] [$cm^3\ g^{-1}$]	V_{micro}[e] [$cm^3\ g^{-1}$]	S_{meso}[e] [$m^2\ g^{-1}$]	d_p[f] [nm]
P	-	100	2.4	0.34	0.30	22	-
DA1	87	-	-	0.36	0.32	28	-
DA1-AT1	91 (79)	-	-	0.44	0.33	121	2
DA1-AT1-AW1	94 (74)	-	-	0.62	0.36	197	3
DA2	79	31	-	0.34	0.29	40	-
DA2-AT1	85 (67)	-	-	0.41	0.28	123	2
DA2-AT1-AW1	93 (62)	-	-	0.47	0.23	223	4
DA2-AT2	78 (62)	18	-	0.66	0.20	330	8
DA2-AT2-AW1	87 (54)	35	-	0.79	0.29	258	10
DA4	81	45	5.5	0.46	0.36	79	-
DA4-AW1	89 (72)	31	-	0.49	0.31	173	3
DA4-AT1	89 (79)	37	3.9	0.47	0.27	177	3
DA4-AT1-AW1	94 (74)	52	4.2	0.61	0.26	292	6

[a]Individual step yield, in grams of solid after treatment per gram of starting material (overall yield with respect to the parent zeolite in brackets); [b]Determined by X-ray diffraction (XRD); [c]Determined by inductively coupled plasma optical emission spectroscopy (ICP-OES); [d]Volume adsorbed at $p/p_0 = 0.99$; [e]t -plot method; [f]Average BJH mesopore size.

Figure 3, yields remained ca. 100% on the *x*-axis, whereas on the *y*-axis yields decreased to ca. 80%. Upon alkaline treatment of the dealuminated zeolites, yields lowered substantially starting from a H_4EDTA molarity >0.07 M. Since mesopores are generated by the partial dissolution of the zeolite, this implies that, to introduce substantial mesoporosity in Y zeolites, a Si/Al ratio of roughly 4 needs to be attained. Possibly, the same ratio needs to be reached to enable the recrystallization process as claimed in a previous report.[36] In the latter patent, a dealumination step using citric acid was required prior to successful alkaline-induced recrystallization. Table SI5 shows that exactly this treatment led to the same yield as DA2 (87%), and concomitant alkaline treatment enabled significant dissolution of the material.

In line with the dissolution pattern, Figure 6b shows that mesopore surface areas exceeding 150 $m^2\ g^{-1}$ were obtained starting from Y zeolites dealuminated using H_4EDTA concentrations >0.07 M. Moreover, the plot illustrates that the highest mesopore surface areas were obtained at 0.1-0.4 M of NaOH. Compared to alkaline treatment on ZSM-5,[31] the mesopore surface areas were attained at relatively high overall yields. The latter is tentatively explained by the relatively low-framework density of FAU (13.3 T atoms nm^{-3}) compared to MFI (18.4 T atoms nm^{-3}),[25] requiring the removal of less atoms to obtain a similar-sized mesopore.

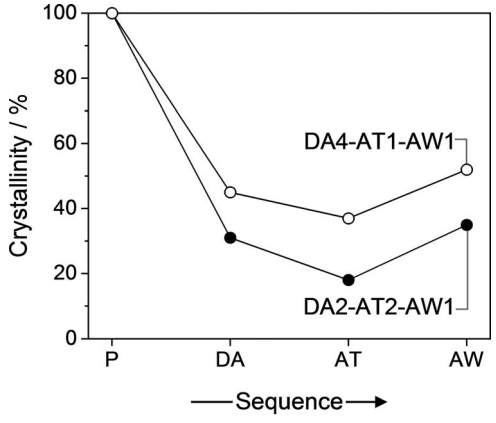

Figure 5. Crystallinity of the Y zeolites at different stages of the sequential treatments. Dealumination (DA) leads to a significant reduction in crystallinity. However, crystallinity is partially recovered after the final acid wash (AW).

High micropore volumes of ca. 0.30 $cm^3\ g^{-1}$ were obtained over a wide variety of conditions (Figure 6c). The reduction of the micropore volume mostly depended on the applied H_4EDTA concentration. Accordingly, marked reductions become apparent only after dealumination with conditions >0.11 M H_4EDTA, whereas the applied alkaline treatment did not affect the obtained values.

Additional efforts, regarding sequential acid and base treatment with aqueous HCl as dealumination agent, proved the value of the H_4EDTA treatment. In the cases HCl was used, the obtained solids exhibited substantial degrees of mesoporosity (up to 234 $m^2\ g^{-1}$), but the micropore volume reduced to zero (Table SI5).

The porosities of the sequentially-treated solids enabled accurate estimation of the average mesopore diameter. Figure 6d shows a variety of pores in the range of ca. 2 to 20 nm as a function of H_4EDTA and NaOH concentration. The highest mesopore surface areas were obtained at pore sizes around 8 nm. When the mesopore size further increased, the mesoporosity dropped, while the total pore volumes remained constant around 0.55 $cm^3\ g^{-1}$ (Table SI4). **Figure 7** highlights the relation between the mesopore diameter and the mesopore surface area for zeolites dealuminated at 0.07 M and 0.11 M H_4EDTA. A volcano plot is obtained with a maximum S_{meso} at 8 nm, displaying a clear relation between the mesopore size and the external surface.

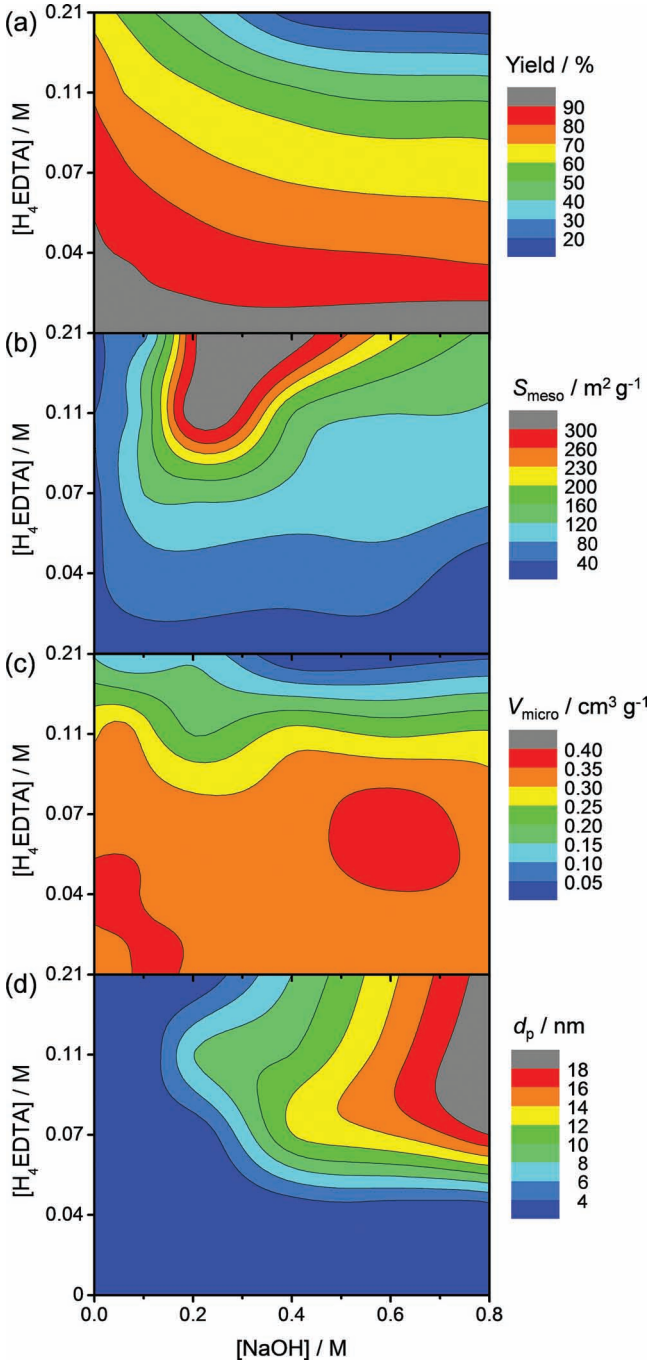

Figure 6. Contour plots obtained by sequential acid and alkaline treatments of the pristine Y zeolite. The effects of concentration of H_4EDTA (y-axis) and NaOH (x-axis) on a) yield, b) S_{meso}, c) V_{micro}, and d) average mesopore size (d_p) are depicted. Hierarchical Y zeolites are obtained at H_4EDTA concentrations exceeding ca. 0.04 M.

2.3. Removal Al-rich Debris from Alkaline-Treated Y Zeolites

The removal of Al-rich debris from alkaline-treated medium-pore zeolites by subsequent acid treatment demonstrated of high value for ZSM-5,[31,37] ferrierite,[38] ZSM-22,[39,40] and theta-1.[41] Reported benefits after the subsequent acid treatment include an enhanced micro- and mesoporosity, increased crystallinity, restored acidity and composition, and, ultimately, enhanced catalytic activity.[31,37–41] The acid washing step was optimized using various concentrations of Na_2H_2EDTA on a number of sequentially acid and base-treated zeolites (Table SI3). For sake of conciseness, discussion is centralized on the results using the treatment of 0.11 M Na_2H_2EDTA (AW1).

Upon Na_2H_2EDTA treatment of the dealuminated and desilicated solids (DAx-ATx), yields reduced with both the severity of the alkaline treatment and the preceding acid treatment (Table 2). Unlike in the case of the samples that were only alkaline treated before washing, the influence of the Na_2H_2EDTA treatment on the physico-chemical properties was more evident. In line with the removal of amorphous Al-rich debris, the crystallinity of DA2-AT2 increased from 18% to 35% (DA2-AT2-AW1, Figure 5). The nitrogen isotherms of the washed samples show that the uptake at $p/p_0 < 0.1$, as well as at middle-to-high relative pressures, increased markedly (Figure 4). The mild acid treatment resulted in the clearing of porosity, leading to increased pore volumes (Table 2). For example, upon washing of DA2-AT2, V_{pore} increased from 0.66 $cm^3\ g^{-1}$ to 0.79 $cm^3\ g^{-1}$ (DA2-AT2-AW1). Additionally, the washing increased the average mesopore size distributions distinctly from 8 to 10 nm (DA2-AT2-AW1), which was confirmed by TEM (DA2-AT2 and DA2-AT2-AW1 in Figure 1). In the case of the solids featuring mesopores of 2 nm (DA1-AT1, and DA2-AT1), the Na_2H_2EDTA treatment resulted in average mesopore sizes of 3 nm (DA1-AT1-AW1), and 4 nm (DA2-AT1-AW1). Except for DA2-AT2-AW1, the external surface area of the samples increased (Table 2). Strikingly, including DA2-AT2-AW1, the relation between the mesopore size and the total surface area, as discussed in Section 2.2, holds solidly after the final acid washing (**Figure 7**).

Recently, the desilication efficiency was introduced as a tool to examine the loss of solids upon introduction of mesoporosity by post-synthetic modification.[39] In this work, the desilication efficiencies of the washed samples varied between 5 and 7 $m^2\ g^{-1}\%^{-1}$, which is slightly higher than those for ZSM-5, and should be due to the relatively high overall yields.

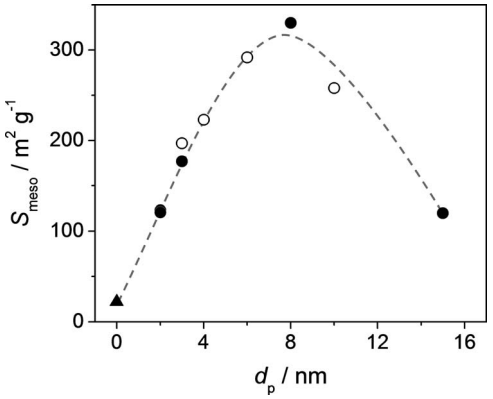

Figure 7. The relation between the average mesopore size (d_p) and the mesopore surface area (S_{meso}) of Y zeolites. The sequentially acid and base-treated samples (DA x-AT x, solid circles), and washed samples (DA x-AT x-AW1, open circles) are derived from Table 2. The parent Y sample is represented by the solid triangle.

The scale up of the preparation of mesoporous zeolites by desilication has been demonstrated on the multiple-liter scale,[42] and more recently on the cubic meter scale.[43] However, these works concerned only a single alkaline treatment on MFI zeolites. In an assessment of reproducibility, we have successfully scaled up all 3 sequential treatments by a factor of roughly 50. Table SI6 shows samples required to prepare sample DA7-AT1-AW1 starting from either 5 or 100 g of parent Y zeolite. Independent on the scale of the various treatments, yields and the resulting porosities are highly comparable, revealing the remarkable scalability of the preparation of mesoporous zeolites by post-synthetic modifications.

2.4. Structure, Porosity, and Morphology of Y Zeolites

For the acidity studies and catalytic evaluation (described in Section 2.5), samples required transformation to the protonic form. It is known that *ex situ* protonation of zeolites can lead to the partial collapse of Y zeolites due to readsorption of water.[26] We have nevertheless employed the latter approach since our catalytic application prevented to do so otherwise. Since samples that were treated at longer dealumination times (24 or 72 h) exhibited a greater stability upon thermal activation (Supporting Information, Figure SI2), we selected sample DA4 (treated for 72 h) for further study.

The sequential treatments (DA4, AT1, and AW1) resulted in similar yields compared to what was described in previous sections (Table 2). Dealumination led to a substantial reduction (55%) of the crystallinity, but not as pronounced as for DA2 (Figure 5). Table 2 shows that, as can be alluded from ref. 34, the Si/Al ratio of 2.4 (P) increased to 5.5 (DA4), implying that about half of the Al was removed from the sample. A subtle difference of the porous properties of DA4 compared to DA2 was revealed by the N_2 isotherm (Figure 4). The uptake at $0.1 < p/p_0 < 0.3$ was more pronounced, suggesting the presence of small mesopores, which were also noticeable in the mesopore size distributions. This difference is attributed to the prolonged reaction time, enabling a more thorough healing of the crystal through Si migration.[44] TEM showed that DA4 did not possess the homogeneity evidenced by the parent zeolite, but the existence of small mesopores could not be ascertained (DA4 in Figure 1). Upon acid wash of the dealuminated sample (to yield sample DA4-AW1), much like after the alkaline treatment, significant mesoporosity was formed ($S_{meso} = 173\ m^2\ g^{-1}$). However, transmission electron microscopy suggested that the porosity is not as homogeneously distributed (DA4-AW1 in Figure 1) and crystallinity decreased from 45% to 31% (Table 2).

Upon desilication of DA4, resulting in DA4-AT1, crystallinity reduced slightly down to 37%, confirming the minimal influence of the alkaline-treatment on the zeolite structure. The Si/Al ratio reduced to 3.9, ratifying the preferential leaching of silicon from the solid. Moreover, Figure 4 reveals that the uptake is shifted to higher relative pressures, indicative of larger mesopores. Accordingly, the mesopore size distribution shows an average pore size around 3 nm, and an S_{meso} of 177 $m^2\ g^{-1}$ is obtained (Table 2). TEM clearly demonstrated the presence of intra-crystalline mesoporosity (DA4-AT1 in Figure 1). The following mild acid washing (DA4-AT1-AW1) resulted in the removal of Al-rich debris, as was substantiated by the increased Si/Al ratio (to 4.2), crystallinity (to 52%), and mesopore size (to 6 nm). The increase in mesopore size was corroborated by TEM (DA4-AT1-AW1 in Figure 1). The mesoporosity increased to 292 $m^2\ g^{-1}$, which was coupled to a micropore volume of 0.26 $cm^3\ g^{-1}$. We conclude that the dealumination treatment leads a partially defective crystal comprising small mesopores clogged with amorphous aluminosilicate debris. The removal of these species is most efficient applying first an alkaline treatment followed by treatment with a mild acid wash. This preferential order could be related to the realumination process that occurs upon alkaline treatment, leading to the reinsertion of Al in the framework.[45–46] We attribute the minimal drop of crystallinity upon alkaline treatment to both the removal of amorphous Si debris and the removal of Si from the framework. The sequential alkaline treatment-acid wash potentially represents a suitable tool to remove aluminosilicate debris from zeolites in general.

Hg porosimetry was measured on P and DA4-AT1-AW1 to monitor the influence on the accessibility of the porous structure (Supporting Information, Figure SI3). Compared to P, the recorded intrusion curve of DA4-AT1-AW1 revealed a strongly enhanced uptake at pressures around 10 bar, which is attributed to a more accessible inter-crystalline porosity.[47] The latter is tentatively explained by a partial deagglomeration of the particles. However, further studies, e.g., complementary microscopic techniques, are required to ascertain this. On the other hand, whereas the parent zeolite did not display uptake at $P > 10$ bar, the hierarchical zeolite showed enhanced uptake in the 1000-4000 bar pressure range, indicative of the presence of *connected* intra-crystalline mesopores. These measurements support the mesopore size determined by N_2 sorption.

2.5. Acidity, Adsorption, and Catalytic Evaluation of Y Zeolites

Conversion to the protonic form (code 'H') by thermal activation led to the partial amorphization of the solids (Table SI7). The drop in crystallinity was about 40% for all samples. Nevertheless, the porous properties remained largely intact. The mesoporous sample of highest interest (DA4-AT1-AW1) displayed a reduction in micropore volume from 0.26 $cm^3\ g^{-1}$ to 0.19 $cm^3\ g^{-1}$, whereas the mesopore surface area decreased from 292 to 202 $m^2\ g^{-1}$. ^{27}Al MAS NMR revealed that in all calcined samples, the majority of aluminum was present in a tetrahedral coordination (Supporting Information, Figure SI4).

Acidity assessment was performed by infrared spectroscopy performed in the OH stretching region (**Figure 8**) and by temperature programmed desorption of ammonia (Supporting Information, Figure SI5). IR spectroscopy was undertaken to study the hydroxyls related to Brønsted acidity (3600 and 3550 cm^{-1}) and those representative of isolated silanols on the external surface (3740 cm^{-1}).[48] The parent Y zeolite displayed mainly the bands related to Brønsted acidity, attending to its high acidity and limited external surface area. Upon dealumination (DA4-H) the bands related to the Brønsted acidity became less intense, which should be related to the lower Al content and the formation of Al-rich debris, respectively. On the other hand, the band at 3740 cm^{-1} became prominent, corroborating the presence of substantial

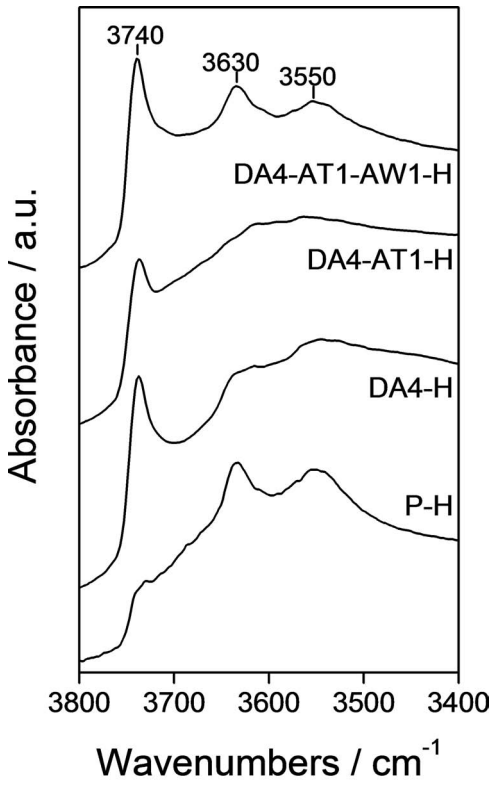

Figure 8. Infrared spectra in the OH stretching region of Y zeolites.

defects. Sequential alkaline treatment (DA4-AT1-H) led to a strong reduction in intensity and definition of the three bands. The latter relates to the realumination of the surface.[31,49] Upon subsequent acid wash (DA4-AT1-AW1-H), the intensity and definition of all bands increased strongly again, attending to the removal of Al-rich debris, confirming the strong suppressive effect on the bands in the OH stretching region. Using NH_3-TPD a more conclusive idea of the bulk acidity was provided (Supporting Information, Figure SI5). The total acidity of the samples, as estimated from the integral of the curves, related well to their Al content. It is clear that these samples deserve more in-depth acidic characterization by, for example, infrared spectroscopy of adsorbed CO and alkyl pyridines. These studies, however, are beyond the scope of this contribution.

Toluene adsorption was measured on selected hierarchical Y zeolites (**Figure 9**). In line with the mostly microporous character of unmodified Y zeolites, the parent sample (P-Na) displayed a major uptake at low relative pressures, while uptake at higher relative pressures was mostly absent. The total uptake of toluene was ca. 2.5 mmol g^{-1}. The hierarchical sample in sodium form (DA4-AT1-AW1-Na) displayed an uptake of ca. 1.5 mmol g^{-1} at $p/p_0 < 0.1$, and an additional 2 mmol g^{-1} at higher relative pressures due to the presence of intra-crystalline mesopores. The total uptake was ca. 3.5 mmol g^{-1}, i.e., 70% higher than that of P-Na.

Catalytic evaluation was performed by the liquid-phase alkylation of benzyl alcohol with toluene. This reaction benefited dramatically from the introduction of mesoporosity by desilication in the case of ZSM-5.[31] However, since the FAU micropores

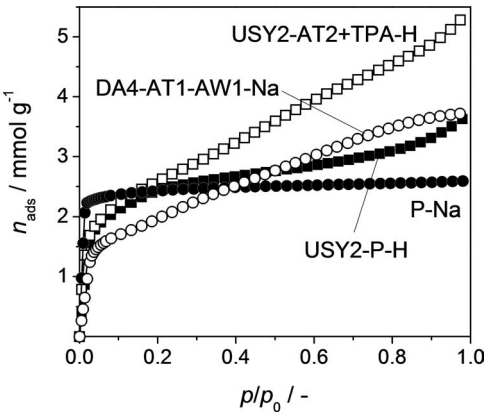

Figure 9. Toluene adsorption isotherms at 298 K of parent and hierarchical Y and USY zeolites.

are, for toluene and benzyl alcohol, more accessible than the ZSM-5 micropores, it is the question whether the catalytic performance of the already very active Y zeolite is improved by the post-synthetic modifications. **Figure 10**a shows the catalytic conversion as a function of time for selected zeolites. The performance of the parent zeolite (P-H) displayed a 47% conversion of benzyl alcohol (X_{BA}) after 40 min. Upon introduction of mesoporosity by sequential dealumination and desilication (DA4-AT1-H), a slightly higher activity was achieved (X_{BA} = 53% after 40 min). Conversely, after the final wash (DA4-AT1-AW1-H), the activity almost doubled after 40 min of reaction (X_{BA} = 84% after 40 min). Upon normalizing the conversion to the Al content, the differences between the samples became even more obvious. The activity of DA4-AT1-AW1-H was almost four-fold of that of P-H, and over two times that of DA4-AT1-AW1-H. We attribute the improved catalytic activity to the improved access to the acid sites provided by the introduced secondary porosity. It can be concluded that the introduction of external surface area is mostly efficient if accessible, hence connected to the external surface, and free of non-zeolitic debris.

2.6. Hierarchical USY Zeolites

2.6.1. USY

In Sections 2.1-2.3 the introduction of mesoporosity in a pristine Y zeolite was tackled. However, it is unclear if the followed approach also holds for a Y zeolite that was steamed, i.e., a USY faujasite with similar bulk Si/Al ratio but higher framework Si/Al ratio. We performed alkaline treatments on a steamed zeolite (USY1-P) using different NaOH concentrations. The results, listed in **Table 3**, indicate that, like in the case of the pristine Y zeolite, relatively mild treatments (0.2 M NaOH, USY1-AT2) do not lead to any apparent modification of the solid. Only at higher concentrations (>1 M NaOH) dissolution occurred, displaying yields down to 17% (USY1-AT4). Upon treatment of USY1 at higher alkalinities, microporosity reduced drastically. The latter is attributed to the realumination of the extra-framework Al (generated by steaming) upon alkaline treatment. This suggests that the direct desilication of USY is not the right strategy.

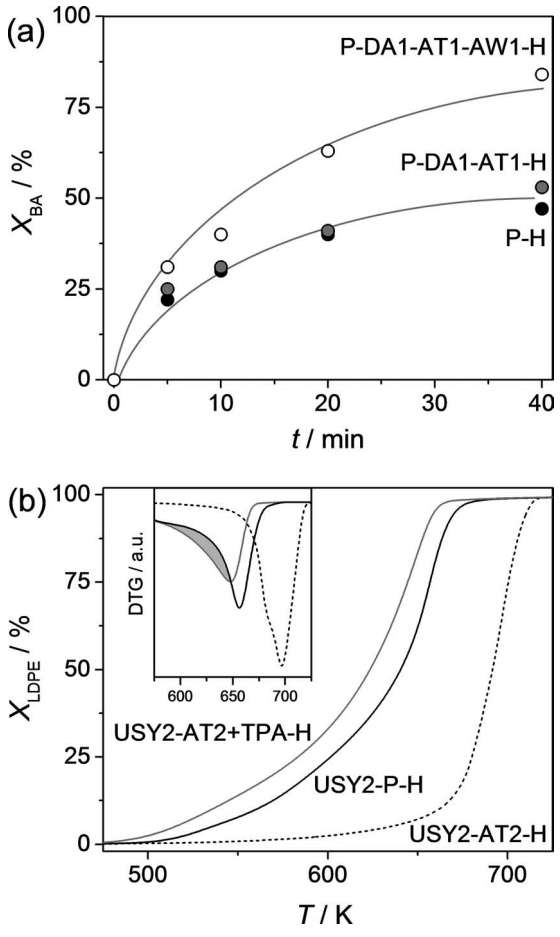

Figure 10. Catalytic evaluation of Y and USY zeolites in a) the alkylation of toluene with benzyl alcohol and b) the pyrolysis of low-density polyethylene. Inset in (b): derivative of the thermo-gravimetric (DTG) profiles. The grey area in the inset highlights the increased light-off of sample USY2-AT2+TPA-H.

To successfully introduce intra-crystalline mesoporosity, we applied the protocol established for the pristine Y zeolite on USY1-P. The resulting solid (USY1-DA3-AT1-AW1) displayed an impressive mesopore surface area (296 m^2 g^{-1}), and a micropore volume of 0.13 cm^3 g^{-1} (Table 3). Accordingly, it is clear that, like in the case of pristine Y, steamed zeolites are also readily prepared in hierarchical form by desilication once the Si/Al ratio has been increased by mild dealumination. However, despite the large external surface increase, both acid treatments (DA3 and AW1) led to a reduction of the micropore volume. Additionally, although the mesopore surface area and the pore volume increased, the crystallinity of USY1-DA3-AT1-AW1 was similar to that of USY1-DA3-AT1.

2.6.2. Dealuminated USY

A remarkable result is the large difference in dissolution kinetics of pristine and dealuminated Y zeolite upon alkaline treatment. As mentioned in the Introduction, the facile dissolution is particularly pronounced for zeolites which were severely dealuminated. The high sensitivity of the FAU topology to alkaline media should relate to the relative low framework density, high surface area, and large micropores (all of which are tightly interconnected).[25] Of course, whereas the application of mild conditions is economically and environmentally favorable, the associated amorphization of the material, as evidenced by de Jong et al.,[33] is undesired.

Recently, we demonstrated that addition of tetraalkylammonium cations in the alkaline solution protects the zeolite crystals during the demetallation process.[50] Using this concept, we executed alkaline treatments on steamed and severely dealuminated USY zeolites (Si/Al = 15, coded 'USY2-P' and Si/Al = 30, coded 'USY3-P') in the *absence* and in the *presence* of TPA^+. **Figure 11**a shows that, upon conventional alkaline treatment of USY2, the N_2-isotherm displayed increased uptake at middle-to-high relative pressures and mesopore surface areas up to 275 m^2 g^{-1} were obtained (USY2-AT1, Table 3). However, the uptake at $p/p_0 < 0.1$ decreased strongly, indicating a significant amorphization of the material. Indeed, V_{micro} dropped from 0.28 cm^3 g^{-1} (USY1-P) down to 0.10 cm^3 g^{-1} (USYY2-AT1). The 65% loss of micropore volume was accompanied with a similar loss in crystallinity (62%, Table 3). The more amorphous appearance of the crystals was confirmed by TEM (Figure 11b).

When TPA^+ was included in the alkaline solution, the resulting solids showed dramatically improved structural and textural properties. Sample USY2-AT2+TPA displayed a similar uptake at $p/p_0 > 0.1$ compared to USY2-AT1, but the uptake at low relative pressures was fully preserved with respect to USY2-P (Figure 11a). Accordingly, the textural properties indicate a V_{micro} of 0.29 cm^3 g^{-1} and a S_{meso} of 253 m^2 g^{-1}. Moreover, the crystallinity loss upon treatment was limited to 37% (Table 3).

When the same treatments were applied to USY3, the positive influence of TPA^+ in the alkaline solution was even more striking. The solids exposed to the standard desilication protocol combined the development of external surface area (up to 321 m^2 g^{-1} for USY3-AT2) with a drastic loss of the micropore volume (0 for USY3-AT2). In contrast, when TPA^+ cations were present in the alkaline solution, V_{micro} remained mostly unaffected, while strongly enhanced V_{pore} (up to 1.10 cm^3 g^{-1} for USY3-AT2+TPA) and S_{meso} (up to 500 m^2 g^{-1} for USY3-AT2+TPA) were attained (Figure 11c, Table 3). Undoubtedly, the protective role displayed on MFI[30,50] is also effective for FAU. Therefore, the use of pore-growth moderators during desilication should be particularly efficient for framework comprising large micropores and/or large surface areas.

2.6.3. Adsorption and Catalytic Evaluation

Gravimetric adsorption of toluene was also performed on USY2-P and USY2-AT2+TPA (Figure 9). At low relative pressures ($p/p_0 < 0.1$), USY2-P displayed an uptake of ca. 2 mmol g^{-1}, which was combined with an additional uptake of 1.5 mmol g^{-1} at higher relative pressures. The latter relates to the microporous nature of the zeolite and the presence mesoporosity (S_{meso} = 125 m^2 g^{-1}). The isotherm of the treated zeolite (USY2-AT2+TPA) displayed a similar uptake at lowest relative pressures, indicative of the preservation of the intrinsic zeolite properties. Furthermore, a strongly increased uptake at

Table 3. Treatment yields and properties of USY zeolites.

Sample	Yield[a] [%]	Crystallinity[b] [%]	V_{pore}[c] [$cm^3\ g^{-1}$]	V_{micro}[d] [$cm^3\ g^{-1}$]	S_{meso}[d] [$m^2\ g^{-1}$]
USY1-P	-	79	0.41	0.30	74
USY1-AT2	100	-	0.36	0.26	49
USY1-AT3	69	-	0.28	0.10	47
USY1-AT4	17	-	0.07	0	12
USY1-DA3	84	30	0.30	0.20	60
USY1-DA3-AT1	64 (54)	21	0.51	0.21	214
USY1-DA3-AT1-AW1	80 (43)	20	0.60	0.13	296
USY2-P	-	63	0.51	0.28	125
USY2-AT1	82	24	0.52	0.10	275
USY2-AT2	54	-	0.28	0.04	203
USY2-AT1+TPA	76	-	0.58	0.28	164
USY2-AT2+TPA	65	39	0.71	0.29	253
USY3-P	-	-	0.61	0.33	117
USY3-AT1	77	-	0.47	0.05	291
USY3-AT2	44	-	0.58	0	321
USY3-AT1+TPA	71	-	0.71	0.29	236
USY3-AT2+TPA	47	-	1.10	0.26	500

[a]Yield in grams of solid after treatment per gram of starting material (overall yield with respect to the parent zeolite in brackets); [b]Determined by X-ray diffraction. Values are relative to parent Y zeolite (P); [c]Volume adsorbed at $p/p_0 = 0.99$; [d]t -plot method.

$p/p_0 > 0.2$ was discerned, which is attributed to the introduced mesoporosity. The total uptake of the aromatic probe molecule was about 5 mmol g^{-1}, i.e., 1.5-fold that of the untreated USY2 zeolite.

The pyrolysis of low-density polyethylene (LDPE) was investigated as it forms a simple test for diffusion-limited reactions.[38,51–52] Figure 10**b** shows the conversion of LDPE (X_{LDPE}) to volatile compounds as a function of temperature in presence of USY zeolite catalysts. The conversion profile of USY2-P-H displayed a temperature at which 10% LDPE is converted (T_{10}) of 560 K, which is significantly lower than the non-catalyzed degradation of LDPE (T_{10} = 710 K). The hierarchical sample (USY2-AT2+TPA-H, T_{10} = 530 K) displayed a significantly higher activity than the parent zeolite, which is attributed to the more accessible micropore structure. In contrast, USY2-AT2-H evidenced, with a T_{10} of 650 K, a much lower activity than the parent zeolite. This confirms that, upon introducing secondary porosity, the intrinsic zeolite properties should remain mostly preserved.

2.7. Strategies for the Preparation of Hierarchical FAU

Clearly, the introduction of mesoporosity in Y or USY zeolites by post-synthetic modification requires careful selection of the strategy (**Figure 12**). On the one hand, the pristine Al-rich zeolite is highly resistant to alkaline solutions, while on the other hand, the high-Si analogue is extremely sensitive in alkaline media. Hence, the starting zeolite (pristine or steamed) should either be mildly or severely dealuminated, the choice of which should depend on the requirements of the final application. When a mild dealumination is applied, the resulting zeolite should be exposed to a sequential alkaline treatment and acid wash to remove the abundant aluminosilicate debris. In the case of high-Si zeolites, the sequential alkaline treatment requires the inclusion of a pore-growth moderator, e.g., TPA^+.

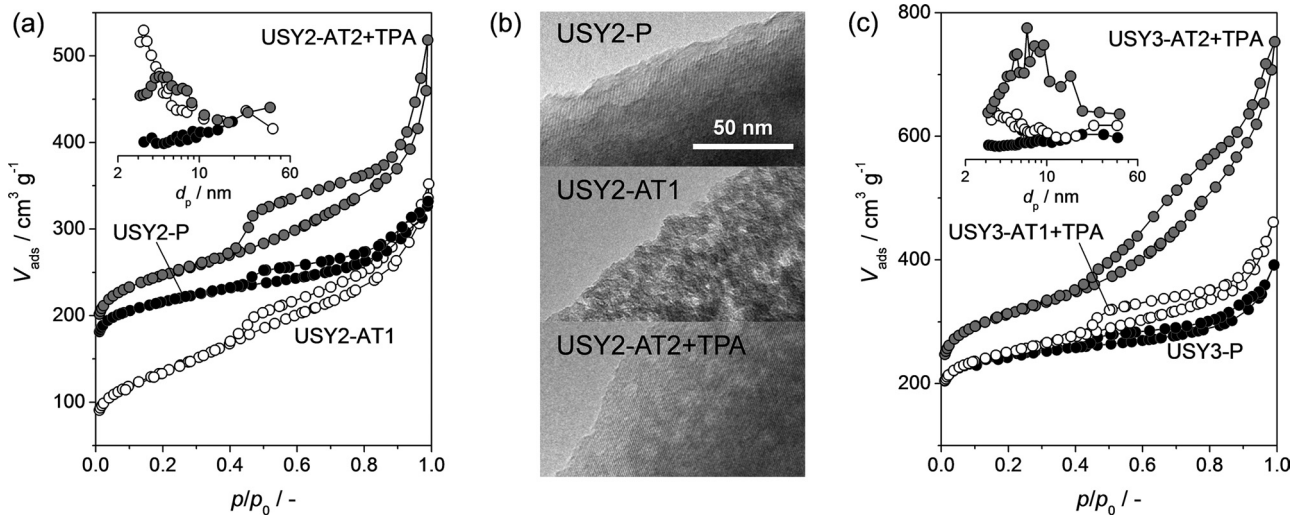

Figure 11. a,c) N_2 isotherms at 77 K and b) transmission electron micrographs of treated Si-rich USY zeolites ('USY2' and 'USY3'). The scale bar in (b) applies to all images. Inset in (a) and (c): BJH mesopore size distributions. The presence of tetrapropylammonium cations (USY2-AT2+TPA, USY3-AT1+TPA, USY3-AT2+TPA) in the NaOH solution leads to a more controlled zeolite dissolution, and accordingly to the preservation of microporosity and crystallinity upon mesopore formation.

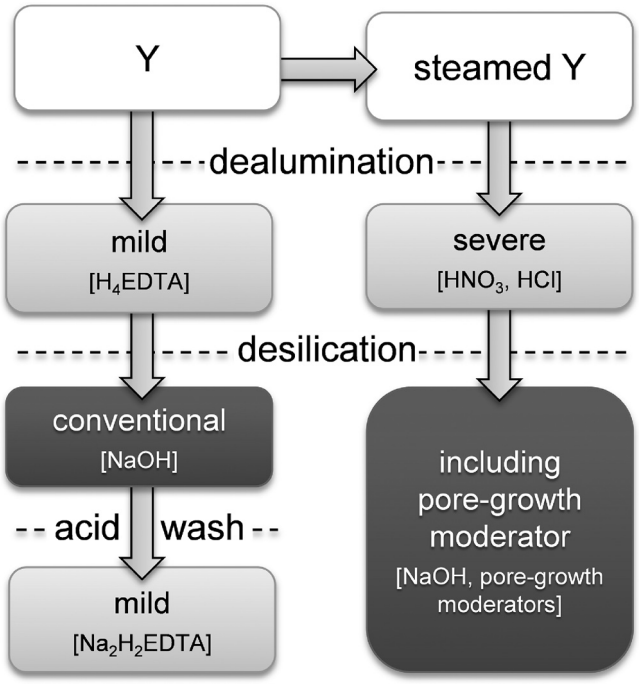

Figure 12. Strategies to design hierarchical FAU zeolites by post-synthetic modifications. After desilication of Al-rich zeolites, the removal of remaining debris by a mild acid wash is crucial. On the other hand, upon alkaline treatment of Si-rich zeolites, the inclusion of pore-growth moderators is highly beneficial.

Of course, the combination of the two, i.e., both inclusion of pore-growth moderators in the alkaline solution and application of the acid wash, are feasible too.

We expect that the preparation of hierarchical Y and USY zeolites by post-synthetic modifications will have a large impact on catalytic processes associated with bulky reagents and/or fast deactivation. Accordingly, their catalytic superiority in traditional reactions, like fluid catalytic cracking and hydrocracking, is anticipated. Moreover, this novel family of hierarchical faujasites might be promising in the conversion of biomass, since these reactions often take place in viscous aqueous media prone to suffer from diffusional constraints.[3,4]

3. Conclusions

Combinations of post-synthetic modifications, including base (NaOH) and acid (H_4EDTA and Na_2H_2EDTA) treatments, were strategically applied to prepare a wide variety of hierarchical Y and USY zeolites. It was demonstrated that both the pristine Y and its steamed ultra-stable derivative USY need to be carefully dealuminated to facilitate subsequent introduction of mesoporosity by desilication in alkaline medium. It proved of vital importance to remove Al-rich debris after sequential acid and base treatment of Y and USY zeolites with low Si/Al ratios, freeing porosity, and increasing crystallinity. The sequential alkaline treatment and acid wash concomitantly remove amorphous aluminosilicates debris formed after framework dealumination of zeolites. For Al-deficient zeolites, the inclusion of TPA^+ in the alkaline solution plays a vital role moderating Si dissolution, yielding a hierarchical USY zeolite with preserved crystallinity and microporosity. The latter strategy should particularly benefit the introduction of mesoporosity by desilication in zeolites of low framework density and low Al content. The superiority of the hierarchical Y and USY zeolites was demonstrated in the adsorption of toluene, the alkylation of benzyl alcohol with toluene, and the pyrolysis of LDPE. Our results emphasize that, in principle, each zeolite can be prepared in hierarchical form, provided that both the individual post-synthetic treatments, as well as the sequences hereof, are optimized.

4. Experimental Section

Materials and Procedures: The zeolites used in this study were provided by Zeolyst International, and are derived from the same NaY zeolite, i.e., CBV100. As a starting material for the majority of the post-synthetic modifications, zeolite Y (CBV300, NH_4-form, nominal Si/Al = 2.6) was used. This sample is coded "P" (parent or pristine). The prefixes "USY1-", "USY2-", and "USY3-" were used for treatments performed on steamed (CBV500, NH_4-form, nominal Si/Al = 2.6) and severely steamed + dealuminated (CBV720, H-form, nominal Si/Al = 15, and CBV760, H-form, nominal Si/Al = 30) USY zeolites, respectively.

Post-synthetic modifications, using aqueous solutions of H_4EDTA, Na_2H_2EDTA, citric acid, HCl, NaOH, and TPAOH, were performed using the conditions mentioned in Table 1 and Table SI1. Treatments using volumes of up to 100 cm^3 were performed under magnetic stirring using an Easymax™ 102 instrument from Mettler Toledo. Treatments involving solutions of 100-500 cm^3 were executed under magnetic stirring in round-bottomed flasks equipped with reflux condensers. Experiments involving volumes > 500 cm^3 were performed in a Büchi miniPilot 5 reactor under mechanical stirring. In a typical experiment, the zeolite sample (0.3-100 g) was added to a vigorously stirred solution of the desired solute, molarity (0.04-5 M), and temperature (338 or 373 K), and was left to react for the required time (0.5-72 h). Afterwards, the reaction was quenched and the resulting solid was filtered, washed using distilled water, and dried overnight at 338 K.

Treatments were performed using 6.7 g zeolite per 100 cm^3 (H_4EDTA and Na_2H_2EDTA), 10 g per 100 cm^3 (citric acid), and 3.3 g per 100 cm^3 (NaOH and HCl). Experiments using H_4EDTA, citric acid, or HCl were labeled 'DA*x*' (DA: dealumination). Na_2H_2EDTA treatments were coded "AW*x*" (AW: acid wash). NaOH treatments were labeled "AT*x*" (AT: alkaline treatment), while those involving both NaOH and TPAOH were named "AT*x*+TPA". In all cases, the suffix "*x*" represents integers for further specification.

In the case TPAOH was present in the alkaline solution, a calcination in static air at 723 K for 5 h using a heating rate 5 K min^{-1} was applied after treatment to remove adsorbed TPA^+ species. Selected zeolites were brought in the protonic form (code 'H') by 3 consecutive ion exchanges in 0.1 M NH_4NO_3 (298 K, 8 h, 1 g zeolite per 100 cm^3 of solution), followed by the abovementioned calcination protocol. Samples brought to the sodium form, by 3 consecutive ion exchanges in 0.1 M $NaNO_3$ (298 K, 8 h, 1 g zeolite per 100 cm^3 of solution), were coded "Na".

Characterization: Transmission electron microscopy (TEM) imaging was performed with a Phillips CM12 instrument operated at 100 kV. A few droplets of the samples suspended in methanol were placed on a carbon-coated copper grid, followed by evaporation at ambient conditions. Nitrogen adsorption at 77 K was performed in a Quantachrome Quadrasorb-SI gas adsorption analyzer. Prior to the measurement, the samples were degassed in vacuum at 573 K for 3 h. The *t*-plot method was used to discriminate between micro- and mesoporosity. The mesopore size distribution was obtained by the Barrett-Joyner-Halenda (BJH) model applied to the adsorption branch of the isotherm. Mercury intrusion porosimetry experiments were performed on a Micromeritics Autopore IV 9510, which operated in the pressure range from vacuum to 4000 bar. Degassing was undertaken in situ. A contact angle of 140° for mercury and a cylindrical

pore model were used to derive the corresponding pore size distribution. Powder X-ray diffraction (XRD) patterns were acquired in a PANanalytical X'Pert PRO-MPD diffractometer equipped with Bragg-Brentano geometry and Ni-filtered Cu Kα radiation ($\lambda = 0.1541$ nm). Data were recorded in the 2θ range of 3–60° with an angular step size of 0.05° and a counting time of 8 s per step. The variation in zeolite crystallinity resulting from post-synthetic modifications was derived from the relative intensity of the (533) reflection at 24° 2θ, assuming 100% crystallinity in the parent sample. The reproducibility of the crystallinity analysis was within 5%. Si and Al concentrations in the solids were determined by inductively coupled plasma optical emission spectroscopy (ICP-OES) on a Horiba Ultra 2 instrument equipped with photomultiplier tube detection.[27] Al magic angle spinning nuclear magnetic resonance (MAS NMR) spectroscopy was performed at a spinning speed of 10 kHz on a Bruker Avance 400 NMR spectrometer equipped with a 4 mm probe head and 4 mm ZrO_2 rotors at 182.4 MHz. Spectra were obtained using 2048 accumulations, 90 pulses with a pulse length of 2.4 µs, a recycle delay of 0.25 s, and with $(NH_4)Al(SO_4)_2{\cdot}12H_2O$ as a reference. Fourier transform infrared (FTIR) spectroscopy was carried out in a Thermo Nicolet 5700 spectrometer equipped with a SpectraTech Collector II diffuse reflectance (DRIFT) accessory and a high-temperature cell, KBr windows, and a MCT detector. Spectra were recorded under a N_2 atmosphere at 473 K, in the range of 650-4000 cm^{-1}, by co-addition of 200 scans and with a nominal resolution of 4 cm^{-1}. Prior to the measurement, the samples were dried at 573 K in N_2 flow (100 cm^3 min^{-1}) for 60 min. Temperature-programmed desorption of ammonia (NH_3-TPD) was carried out in a Thermo TPDRO 1100 unit equipped with a thermal conductivity detector. The zeolite (100 mg) was pre-treated at 573 K in He flow (20 cm^3 min^{-1}) for 3 h. Afterwards, 10 vol.% of NH_3 in He (20 cm^3 min^{-1}) was adsorbed at 473 K for 30 min followed by He purging at the same temperature. This procedure was repeated 3 times, after which the desorption of NH_3 was monitored in the range of 473-973 K (heating rate: 10 K min^{-1}). Adsorption isotherms of toluene were measured at 298 K in an Intelligent Gravimetric Analyzer (IGA-002, Hiden Analytical). The samples (10 mg) were outgassed at 573 K for 3 h prior to measurement. The isotherms were measured by increasing the vapor pressure in the range of 0-38 mbar.

Catalytic Testing: The activity of treated zeolites was tested in the liquid-phase alkylation of toluene with benzyl alcohol using an Endeavor Catalyst System (Argonaut Technologies), consisting of eight parallel reactors with a working volume of 5 cm^3 and with continuous stirring by overhead impellers. The catalysts were activated *ex situ* at 573 K under inert atmosphere, and maintained at this condition for 1 h in order to eliminate adsorbed water. Reaction conditions were T = 413 K, P = 5 bar, molar toluene-to-benzyl alcohol ratio of 80, and a catalyst amount of 40 wt.% of zeolite with respect to the amount of benzyl alcohol. Reaction products were analyzed offline at different reaction times using a gas chromatograph (HP 6890) equipped with a mass selective detector (HP 5973). LDPE (Alfa Aesar) pyrolysis was carried out in a Mettler Toledo TGA/DSC 1 STAR^e System. The polymer (6 mg) and the zeolite (2 mg), both in powder form, were carefully weighed in a 70 µL α-Al_2O_3 crucible and suitably mixed in order to attain an intimate contact. The pyrolysis was performed in N_2 (70 cm^3 min^{-1}) ramping the temperature from 303 to 973 K at 10 K min^{-1}.

Supporting Information

Supporting Information is available from the Wiley Online Library or from the author.

Acknowledgements

ETH Zurich and the Swiss National Science Foundation (project number 200021-134572) are acknowledged for financial support. We thank Dr. S. Mitchell and M. Milina for TEM and toluene adsorption analyses, respectively. This article was amended on March 7, 2012 to include labels in Figure 4c, which were missing in the version originally published online.

Received: October 7, 2011
Published online: December 21, 2011

[1] A. Corma, *Chem. Rev.* **1995**, *95*, 559.
[2] W. Vermeiren, J.-P. Gilson, *Top. Catal.* **2009**, *52*, 1131.
[3] E. Taarning, C. M. Osmundsen, X. Yang, B. Voss, S. I. Andersen, C. H. Christensen, *Energy Environ. Sci.* **2011**, *4*, 793.
[4] R. M. West, M. S. Holm, S. Saravanamurugan, J. Xiong, Z. Beversdorf, E. Taarning, C. H. Christensen, *J. Catal.* **2010**, *269*, 122.
[5] A. Corma, *Chem. Rev.* **1997**, *97*, 2373.
[6] J. Pérez-Ramírez, C. H. Christensen, K. Egeblad, C. H. Christensen, J. C. Groen, *Chem. Soc. Rev.* **2008**, *37*, 2530.
[7] S. van Donk, A. H. Janssen, J. H. Bitter, K. P. de Jong, *Catal. Rev. - Sci. Eng.* **2003**, *45*, 297.
[8] R. Chal, C. Gerardin, M. Bulut, S. van Donk, *ChemCatChem* **2011**, *3*, 67.
[9] S. Lopez-Orozco, A. Inayat, A. Schwab, T. Selvam, W. Schwieger, *Adv. Mater.* **2011**, *23*, 2602.
[10] L. Tosheva, V. Valtchev, *Chem. Mater.* **2005**, *17*, 2494.
[11] W. J. Roth, J. Čejka, *Catal. Sci. Technol.* **2011**, *1*, 43.
[12] J. Čejka, S. Mintova, *Catal. Rev. -Sci. Eng.* **2007**, *49*, 457.
[13] K. Egeblad, C. H. Christensen, M. Kustova, C. H. Christensen, *Chem. Mater.* **2008**, *20*, 946.
[14] D. Verboekend, J. Pérez-Ramírez, *Catal. Sci. Technol.* **2011**, *1*, 879.
[15] M. Choi, H. S. Cho, R. Srivastava, C. Venkatesan, D.-H. Choi, R. Ryoo, *Nat. Mater.* **2006**, *5*, 718.
[16] H. Chen, J. Wydra, X. Zhang, P.-S. Lee, Z. Wang, W. Fan, M. Tsapatsis, *J. Am. Chem. Soc.* **2011**, *133*, 12390.
[17] F. N. Gu, F. Wei, J. Y. Yang, N. Lin, W. G. Lin, Y. Wang, J. H. Zhu, *Chem. Mater.* **2010**, *22*, 2442.
[18] R. Chal, T. Cacciaguerra, S. van Donk, C. Gérardin, *Chem. Commun.* **2010**, *46*, 7840.
[19] M. Choi, K. Na, J. Kim, Y. Sakamoto, O. Terasaki, R. Ryoo, *Nature* **2009**, *461*, 246.
[20] S. Mintova, N. H. Olson, V. Valtchev, T. Bein, *Science* **1999**, *283*, 958.
[21] G. T. Kerr, *J. Phys. Chem.* **1967**, *71*, 4155.
[22] C. J. Plank, E. J. Rosinski, *US3* 257310, **1966**.
[23] R. L. Bedard, *Zeolites in Industrial Separation and Catalysis*, Wiley-VCH, Weinheim, Germany **2002**. pp. 72–73.
[24] T. Tatsumi, *Handbook of Porous Solids*, Wiley-VCH, Weinheim, Germany **2010**. pp. 913–920.
[25] C. Baerlocher, L. B. McCusker, Database of Zeolite Structures, http://www.iza-structure.org/databases/ (accessed December 2011).
[26] H. K. Beyer, *Molecular Sieves*, Vol. *3*, Springer-Verlag, Berlin Germany **2002**. pp. 208–213.
[27] P. Kortunov, S. Vasenkov, J. Kärger, R. Valiullin, P. Gottschalk, M. F. Elía, M. Perez, M. Stöcker, B. Drescher, G. McElhiney, C. Berger, R. Gläser, J. Weitkamp, *J. Am. Chem. Soc.* **2005**, *127*, 13055.
[28] A. H. Janssen, A. J. Koster, K. P. de Jong, *J. Phys. Chem.* **2002**, *106*, 11905.
[29] J. C. Groen, L. A. A. Peffer, J. A. Moulijn, J. Pérez-Ramírez, *J. Mater. Chem.* **2006**, *16*, 2121.
[30] D. Verboekend, J. Pérez-Ramírez, *Chem. Eur. J.* **2011**, *17*, 1137.
[31] D. Verboekend, S. Mitchell, M. Milina, J. C. Groen, J. Pérez-Ramírez, *J. Phys. Chem. C* **2011**, *115*, 14193.
[32] Z. Qin, B. Shen, X. Gao, F. Lin, B. Wang, C. Xu, *J. Catal.* **2011**, *278*, 266.
[33] K. P. de Jong, J. Zečević, H. Friedrich, P. E. de Jongh, M. Bulut, S. van Donk, R. Kenmogne, A. Finiels, V. Hulea, F. Fajula, *Angew. Chem. Int. Ed.* **2010**, *49*, 10074.
[34] G. T. Kerr, *J. Phys. Chem.* **1968**, *72*, 2594.

[35] A. Gola, B. Rebours, E. Milazzo, J. Lynch, E. Benazzi, S. Lacombe, L. Delevoye, C. Fernandez, *Microporous Mesoporous Mater.* **2000**, *40*, 73.
[36] J. Garcia-Martinez, M. M. Johnson, I. Valla, *US* 0196263, **2010**.
[37] C. Fernandez, I. Stan, J.-P. Gilson, K. Thomas, A. Vicente, A. Bonilla, J. Pérez-Ramírez, *Chem. Eur. J.* **2010**, *16*, 6224.
[38] D. Verboekend, R. Caicedo-Realpe, A. Bonilla, M. Santiago, J. Pérez-Ramírez, *Chem. Mater.* **2010**, *22*, 4679.
[39] D. Verboekend, A. M. Chabaneix, K. Thomas, J.-P. Gilson, J. Pérez-Ramírez, *CrystEngComm* **2011**, *13*, 3408.
[40] D. Verboekend, K. Thomas, M. Milina, S. Mitchell, J. Pérez-Ramírez, J.-P. Gilson, *Catal. Sci. Technol.* **2011**, *1*, 1331.
[41] A. Corma, C. Martinez, E. J. Doskocil, G. Yaluris, *EP* 2272939, **2011**.
[42] J. C. Groen, J. A. Moulijn, J. Pérez-Ramírez, *Ind. Eng. Chem. Res.* **2007**, *46*, 4193.
[43] J. Pérez-Ramírez, S. Mitchell, D. Verboekend, M. Milina, N.-L. Michels, F. Krumeich, N. Marti, M. Erdmann, *ChemCatChem* **2011**, *3*, 1731.
[44] G. Kerr, A. W. Chester, D. H. Olson, *Catal. Lett.* **1994**, *25*, 401.
[45] B. Sulikowski, J. Datka, B. Gil, J. Ptaszynski, J. Klinowski, *J. Phys. Chem. B* **1997**, *101*, 6929.
[46] D.-S. Liu, S.-L. Bao, Q.-H. Xu, *Zeolites* **1997**, *18*, 162.
[47] J. C. Groen, S. Brouwer, L. A. A. Peffer, J. Pérez-Ramírez, *Part. Part. Syst. Charact.* **2006**, *23*, 101.
[48] B. Xu, F. Rotunno, S. Bordiga, R. Prins, J. A. van Bokhoven, *J. Catal.* **2006**, *241*, 66.
[49] V. Calsavara, E. Falabella Sousa-Aguiar, N. R. C. Fernandes Machado, *Zeolites* **1996**, *17*, 340.
[50] J. Pérez-Ramírez, D. Verboekend, A. Bonilla, S. Abelló, *Adv. Funct. Mater.* **2009**, *19*, 3972.
[51] J. Pérez-Ramírez, S. Abelló, A. Bonilla, J. C. Groen, *Adv. Funct. Mater.* **2009**, *19*, 164.
[52] D. Verboekend, J. C. Groen, J. Pérez-Ramírez, *Adv. Funct. Mater.* **2010**, *20*, 1441.